ELSEVIER

Journal of Power Sources 107 (2002) 56–60

JOURNAL OF POWER SOURCES

www.elsevier.com/locate/jpowsour

Properties of containing Sn nanoparticles activated carbon fiber for a negative electrode in lithium batteries

Minato Egashira*, Hideyasu Takatsuji, Shigeto Okada, Jun-ichi Yamaki

Institute of Advanced Materials Study, Kyushu University, 6-1 Kasuga-Koen, Kasuga, Fukuoka 816-8580, Japan

Received 12 July 2001; received in revised form 14 September 2001; accepted 18 October 2001

Abstract

Activated carbon fiber (ACF) containing Sn nanoparticles were prepared by impregnation and were investigated as a negative electrode material in lithium batteries. The tin particle size was controlled by selecting an ACF with an adequate surface structure. This Sn/ACF composite cycled versus Li metal showed a first discharge capacity as high as 200 mAh g^{-1} compared to the pristine ACF which showed only 87 mAh g^{-1}. Excellent cyclability with these composites was obtained with ACF BET SSA as large as 2000 m^2 g^{-1} and 30 wt.% Sn.

Keywords: Tin nanoparticle; Activated carbon fiber; Lithium ion battery

1. Introduction

Lithium alloys with Sn and Si have higher energy density than that of pure lithium as negative electrodes in lithium batteries [1,2]. For example, one Sn atom can be inserted in 4.4 lithium atoms. In other words, metallic tin can exhibit the capacity of about 1000 mAh g^{-1}, about three times of that of the graphite negative electrodes. However, these metal negative electrodes suffer significant mechanical disintegration due to the drastic volumetric changes during lithium insertion and extraction [3], which causes a capacity drop after several charge–discharge cycles.

In 1997, Fujifilm Celltech Inc. proposed an amorphous tin oxide-based material as an excellent negative electrode of lithium batteries with high reversible capacity (about 600 mAh g^{-1}) and good cycleability [4]. Though they claimed that the lithium insertion and removal must occur without forming a lithium–tin alloy, a consideration that tin oxide is reduced to a microcrystalline metal state [5] seems more acceptable. The microcrystalline active phase is expected to minimize the mechanical stress that occurs during the insertion of lithium into the metallic phase [2,6–10]. Several studies about the preparation of an alloy negative electrode of tin nanophase and another metallic species have shown the advantage of a nanosize active phase for the cycleability improvement [9,10].

In the present study, Sn nanoparticles were prepared inside the pores of activated carbon fiber (ACF) by impregnation. The nanopores of ACF can provide nanometer-sized tin particles. the aim of this study is to investigate the relationship between the structure of Sn nanoparticles in ACF pores and the characteristics of Sn-impregnated ACFs.

2. Experimental

Pitch-based ACFs (Osaka Gas Co.; BET SSA500, 700, 1000 and 2000 m^2g^{-1}, to be called OG-5A, -7A, -10A and -20A in the text) were used. The average diameter of these fibers were about 10 μm. Impregnation of Sn salt onto ACFs was carried out either in an aqueous solution (0.01 M H_2SO_4) or in methanol, because we suspected that the immersion in an aqueous solution might be insufficient due to the high surface tension of water. The $SnSO_4$ from Wako Chemical was used as a Sn-impregnation source in aqueous solution and $(CH_3COO)_2$ Sn (Aldrich) as a Sn in ethanol. Prescribed amounts of Sn salt, ACF and solvents were stirred for 2 h, and then the solvent was evaporated. The amount of tin salt was fixed so that the content of tin metal was to be 33 wt.% in the final composite, unless otherwise noted. The authors could not obtain yields after the heat-treatment because we could not take out all of product by a furnace. The ACF impregnated Sn salt on its surface was heat-treated at 1273 K under Ar flow. In this study, obtained materials are called Sn-impregnated ACFs.

* Corresponding author. Fax: +81-92-583-7792.
E-mail address: minat206@cm.kyushu-u.ac.jp (M. Egashira).

0378-7753/02/$ – see front matter
PII: S0378-7753(01)00980-6

The negative electrode material cycleability was tested galvanostatically in SS coin cells. Thin films impregnated ACFs were fabricated on Cu foil using 14.2 wt.% of acetylene black and 5 wt.% of binder (polyvinylidene fluoride). Specific gravimetric capacity was based on the total weight of used ACF/Sn-impregnated ACF and AB. Lithium foil was the counter electrode. Both electrodes were cut to 15 mm in diameter. The electrolyte and separator used are: 1M $LiPF_6$ in EC-DMC 1:1 by volume (Tomiyama Pure Chemical Co.) and porous polypropylene (Celgard #2500), respectively. The SS coin cell were assembled in a dry glove box with humidity <10 ppm. The charge–discharge current was 0.5 mA cm^{-2} (otherwise noted), in a voltage window 1.5–0.0 V.

The structure of Sn-impregnated ACFs was characterized by X-ray diffractometer (Rigaku Co., Geigerflex) and by TEM (JEOL Co., JES-100CX; accelerating voltage 80 kV).

3. Results and discussion

3.1. The state of Sn on the ACF surface

Fig. 1 shows the X-ray diffraction patterns of a pristine ACF OG-7A (a) and 33 wt.% Sn-impregnated ACF, made in aqueous (b) and in ethanol (c) solutions. Arrow marks on the profiles (b) and (c) indicate the position of the diffraction peaks of the metallic tin. It can be seen in Fig. 1 that regardless of the media used for impregnation most of the tin salts were converted into metallic tin in the process of heat-treatment. In addition in Fig. 1, the presence of SnO_2 is shown by three small peaks at 26, 34, and 51° very well distinguishable on the (a) difractogram. Assuming that only Sn and SnO_2 are present in the Sn-impregnated ACFs as tin species, the SnO_2/Sn ratio is estimated 4.6 and 6.0 wt.% for the prepared in aqueous and nonaqueous solution ACF, respectively. The tin oxide can be build by the tin particle oxidation from the ambient oxygen. Ignoring the SnO_2 contribution in the Scherrer's equation $D_{200} = 0.9\lambda/b\cos\theta$, where D_{200} is the size of crystalline vertical to the (2 0 0) plane of tin, λ the wave length of the X-ray and b is the half width of the (2 0 0) peak, crystallite sizes 39 and 40 nm were obtained from the tin (2 0 0) peaks in patterns (b) and (c).

Fig. 2 shows the TEM bright field images of tin-impregnated ACF (from ethanol solution). In this image, the dark 20–40 nm spots indicate metallic tin particles. The size of the tin particles is in a good harmony with D_{200} crystallite size obtained from the X-ray diffraction patterns. That means that the size of a tin particle on a tin-impregnated ACF is the same size as one metallic Sn crystallite. Therefore, we can take the D_{200} crystallite size of tin as the tin particle size on tin-impregnated ACFs. Generally, ACFs possess slit-type micropores at their surface and have a narrow pore-size distributions [11]. The pore size of OG-7A distributes ~10 nm and only ~1% of pores distributed around 20–40 nm from the supplier's data. Therefore, the tin particles having 20–40 nm in diameter are not able to exist in the pores of OG-7A unless the pore structures are pulverized. However, such nanoparticles of tin may sinter

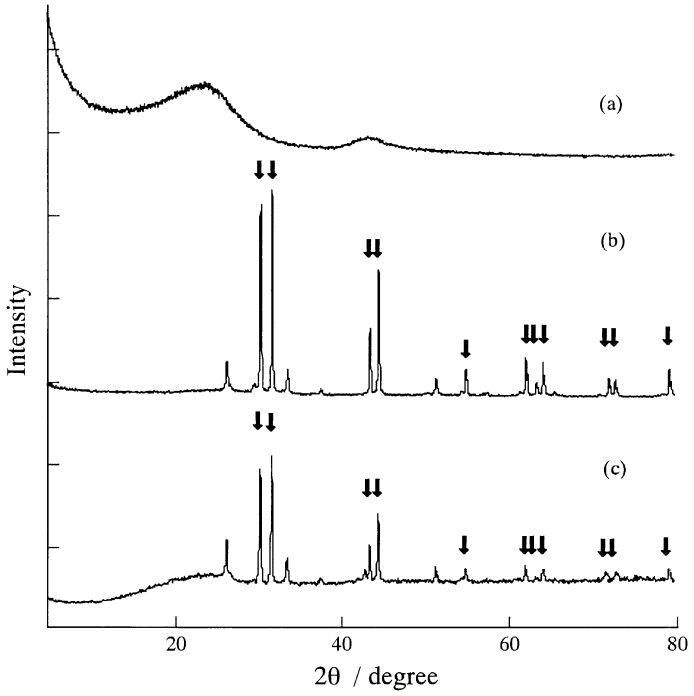

Fig. 1. X-ray diffraction patterns of activated carbon fiber (ACF) and Sn-impregnated ACFs. (a) Pristine OG-7A; (b) Sn-impregnated ACF OG-7A prepared in aqueous solution; (c) Sn-impregnated ACF OG-7A prepared in ethanol solution.

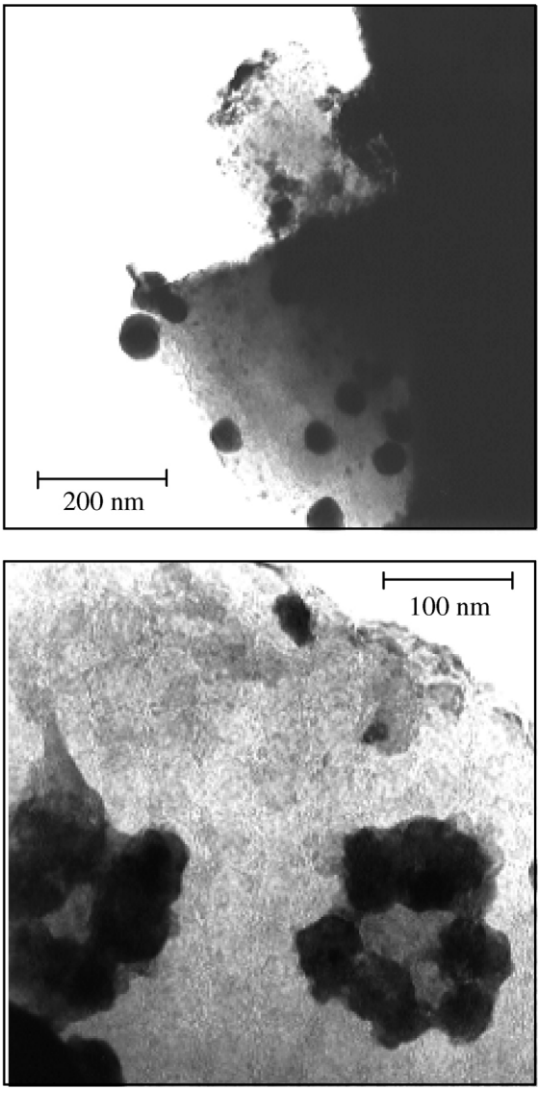

Fig. 2. TEM bright field images of tin-impregnated ACF OG-7A prepared in aqueous solution.

each other if they lie outside of ACF. In the present case, a certain structural factor must prevent tin nanoparticles from sintering.

We also impregnated tin on the surface of ACFs OG-5A, -10A and -20A using a similar method (via aqueous solution). Fig. 3 shows the X-ray diffraction patterns of these tin-impregnated ACFs. Peaks assigned to metallic tin (indicated by arrows in the Fig. 3) are observed in all samples. From the Scherrer equation D_{200} values for the tin-impregnated OG-5A, -7A, -10A and -20A are 43, 39, 34, and 30 nm, respectively. The size of the tin nanoparticles appears to be related to the ACFs pore structure, however, particle sizes are much larger than the average pore sizes of ACFs. It is expected for the pore or surface structure of ACF to affect the tin size nanoparticles. One possible explanation could be that the pore wall burns off during the tin salt reduction on ACF. As a result pore size increases and opens room for the tin particles to grow inside these resulted pores.

3.2. Cycling behaviors of Sn-impregnated ACF negative electrodes for Li cells

Fig. 4 shows first and second charge–discharge profiles of a 33 wt.% tin-impregnated OG-7A prepared via an aqueous and a nonaqueous route. In each profile a plateau appears around 0.4–0.6 V versus Li/Li^+, exhibiting the insertion/extraction process of lithium in the tin species. The initial irreversible capacities of tin-impregnated OG-7A from an aqueous and a nonaqueous route, and of pristine OG-7A can be estimated at 347, 396, and 449 mAh g^{-1}, respectively. Thus, the initial Coulombic efficiencies of these electrodes were calculated to be 35.1, 36.4, and 16.2%, respectively. The impregnation of tin into ACF pores resulted initially in an improved efficiency, however, a significant portion of irreversible capacity remained. Two factors appear to be responsible for this high irreversible capacity. First, this could be due to the lithium adsorption on the ACF surface. Second possibility is the irreversible reduction of SnO_2 by the lithium [5,12–14]. A part of the inserted lithium was consumed by the irreversible adsorption and/or reaction on the ACF surface. This factor also contributed to the first cycle irreversible capacity of tin-impregnated ACFs because the surface of ACF may not be covered completely with tin. Furthermore, the reduction process of tin salt on ACF to tin nanoparticle may bring the increase of surface area of ACF because it must be supplied as a reductant. The content of tin oxide in a tin-impregnated ACF was as small as 2 wt.% and its contribution to the irreversible capacity is small enough and can be ignored.

The reversible extraction of lithium from tin clearly contributed to the additional capacities. The contribution of tin to the reversible capacities of tin-impregnated OG-7A formed via an aqueous or a nonaqueous route was roughly estimated to about 360 and 500 mAh per gram of tin, respectively. We measured also charge and discharge capacities of a tin metal negative electrode under the same experimental condition as tin-impregnated ACFs and obtained a first cycle discharge capacity as small as 170 mAh g^{-1}. Microscopic observations indicated that the tin metal particle size is 20 μm. The current density value was so large that the diffusion of lithium into metallic tin particles was not sufficient for the mixture of tin and OG-7A. The contribution of tin to the reversible capacities of tin-impregnated ACFs seems to be rather large. Nano-size tin particle may help the fast insertion/extraction of lithium. It is expected that the capacity contribution by tin can maintain after 20 cycles because a certain surface structure of ACF holds tin nanoparticle. Moreover, the authors measured X-ray diffraction for the 33 wt.% of tin-impregnated OG-7A (prepared in aqueous solution) after 20 cycles and estimated the crystalline size of tin nanoparticle in it to 33 nm, which is close to the initial tin particle size: 39 nm. This result indicates that the tin nanoparticles were prevented from degradation by certain pore structures of ACF.

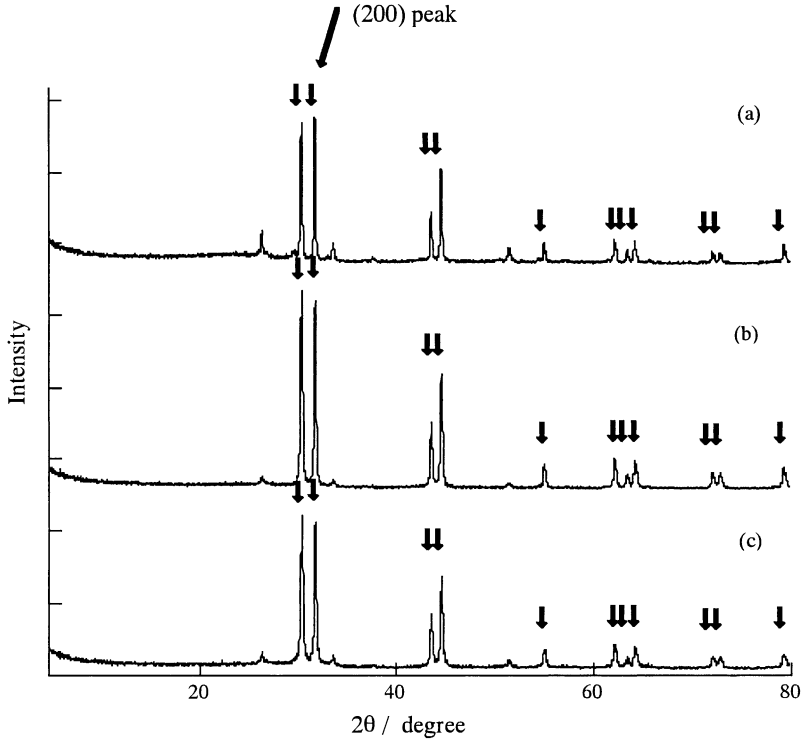

Fig. 3. X-ray diffraction patterns of various Sn-impregnated ACFs. (a) 33 wt.% of Sn-impregnated OG-5A; (b) 33 wt.% of Sn-impregnated OG-10A; (c) 33 wt.% of Sn-impregnated OG-20A.

Fig. 5 shows the first discharge voltage profiles of 33 wt.% of tin-impregnated ACF through an aqueous solution at the constant current densities of 0.5 and 2.0 mA cm^{-2}. As large as 120 mAh g^{-1} of discharge capacity is remained even at the high current density, while the charge–discharge test at 2.0 mA cm^{-1} using graphite electrode resulted the capacity decrease to 1 from 5. The nano-size of tin helped the high rate property of this tin-impregnated ACF.

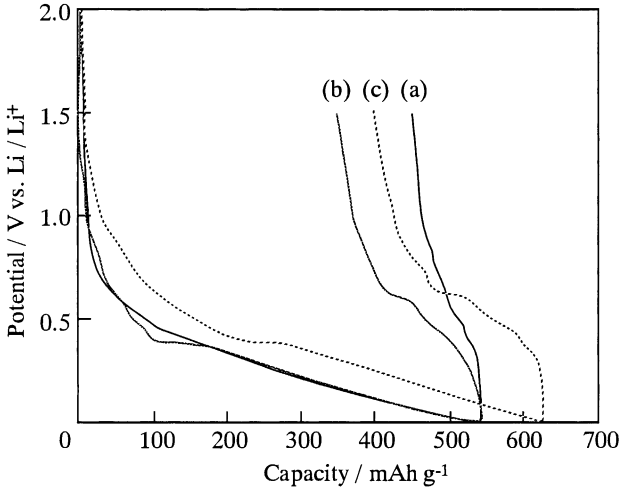

Fig. 4. Voltage profiles at the charge–discharge cycles of Li/Sn-impregnated OG-7A cell. (a) Pristine OG-7A; (b) 33 wt.% of Sn-impregnated OG-7A prepared in aqueous solution; (c) 33 wt.% of Sn-impregnated OG-7A prepared in nonaqueous solution.

Fig. 6 summarizes the discharge cycling behavior of different Sn-impregnated ACF composite negative electrodes. After 20 cycles Sn-impregnated OG-7A prepared via aqueous/nonaqueous route showed higher discharge capacities than pristine OG-7A, despite of the gradually decreased capacity due to the degradation of the tin particles especially prepared in nonaqueous solution. The nonaqueous preparation may provide a larger amount of tin particles, which showed considerable capacity at the first cycle and degraded its reversible capacity during subsequent cycles, on the outer surface of ACF. Tin-impregnated

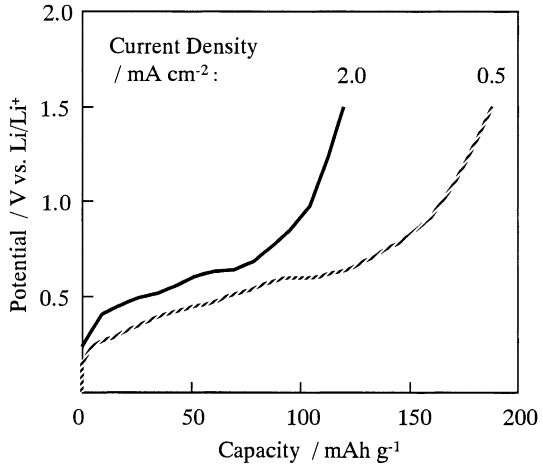

Fig. 5. Voltage profiles at the first discharge cycle of Li/Sn-impregnated OG-7A cell with different discharge current.

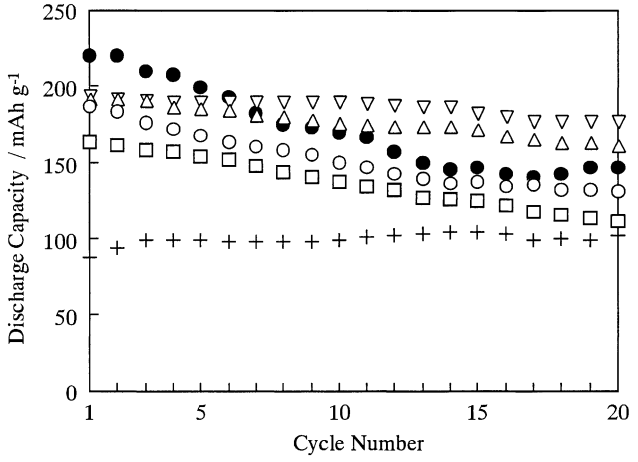

Fig. 6. Specific gravimetric capacity of various Li/Sn-impregnated ACF coin cells after 20 cycles. Symbols: (+), pristine OG-7A; (□), 33 wt.% of Sn-impregnated OG-5A prepared in aqueous solution; (○), 33 wt.% of Sn-impregnated OG-7A prepared in aqueous solution; (●), 33 wt.% of Sn-impregnated OG-7A prepared in nonaqueous solution; (△), 33 wt.% Sn-impregnated OG-10A prepared in aqueous solution; (▽), 33 wt.% Sn-impregnated OG-20A prepared in aqueous solution.

ACF negative electrode is expected to have a good cycle capability when many tin nanoparticles trapped inside the ACF surface structure. Therefore, an ACF with a larger surface area than OG-7A would be expected to have a larger pore volume and to bring a greater number of tin nanoparticles. According to Fig. 6, OG-10A and -20A impregnated with 33 wt.% of tin particles had a greater cycle capability than OG-7A, while OG-5A impregnated with the same amount of tin showed a lower cycle capability. Larger surface area raised the accessibility of tin nanoparticles into the ACF surface structure, and finer nanoparticles also contributed to stabilizing the reversible insertion/extraction of lithium.

In this investigation, the authors do not pretend for having optimized preparation conditions of Sn-impregnated ACFs and using optimum current density for achieving maximum capacity and cycleability for commercialization purposes. However, in the present study the concept of using this kind of composite for an advanced negative electrodes for lithium batteries is successfully proven.

4. Conclusion

Sn nanoparticle/porous carbon composites were prepared by impregnating the surface of porous carbon with a tin salt and subsequent heating. The particle size of metallic tin in this composite was 20–40 nm and was controlled by choosing porous carbon with a appropriate surface structure. Tin nanoparticles existing on an ACF surface provided as high as 100 mAh g^{-1} of additional capacities for the high rate charge–discharge cycle, and showed good cycleability when using adequate Sn amount and ACF the pore volume. Though the reversible capacities are still insufficient at the present level, this kind of composite material is expected to be useful as a negative electrode for advanced lithium batteries by further preparation conditions improvement.

Acknowledgements

The authors thank Dr. Hiroyuki Fujimoto and Dr. Katsuhisa Tokumitsu of Osaka Gas Co., Ltd., for their financial assistance. (Dr. Tokumitsu currently belongs to Shiga Prefectural University.)

References

[1] R.A. Huggins, in: J.O. Besenhard (Ed.), Handbook of Battery Materials, Wiley-VCH, Weinhelm, 1999, p. 359.
[2] M. Winter, J.O. Besenhard, Electrochim. Acta. 45 (1999) 31.
[3] R. Nesper, Prog. Solid State Chem. 20 (1990) 1.
[4] Y. Idota, T. Kubota, A. Matsufuji, Y. Maesaka, T. Miyazaka, Science 276 (1997) 1395.
[5] I.A. Courtney, J.R. Dahn, J. Electrochem. Soc. 144 (1997) 2045.
[6] M. Grätzel, Chem. Tech. 65 (1995) 1300.
[7] J. Morales, L. Sanchez, Solid State Ion. 126 (1999) 219.
[8] J.O. Besenhard, J. Yang, M. Winter, J. Power Sources 68 (1997) 87.
[9] J. Yang, Y. Takeda, N. Imanishi, T. Ichikawa, O. Yamamoto, J. Power Sources 79 (1999) 220.
[10] A.M. Wilson, J.R. Dahn, J. Electrochem. Soc. 142 (1995) 326.
[11] H. Juntgen, Carbon 15 (1977) 273.
[12] T. Brousse, R. Retoux, U. Horterich, D.M. Schleich, J. Electrochem. Soc. 145 (1998) 1.
[13] S. Marchell, T. Shodai, Y. Sakurai, J. Yamaki, J. Power Sources 73 (1998) 216.
[14] R.A. Huggins, J. Power Sources 82 (1999) 13.